NASA Technical Memorandum 106009

P. 14

Modal Element Method for Scattering of Sound by Absorbing Bodies

Kenneth J. Baumeister
Lewis Research Center
Cleveland, Ohio

and

Kevin L. Kreider
The University of Akron
Department of Mathematical Sciences
Akron, Ohio

Prepared for the
The American Society of Mechanical Engineers
Winter Annual Meeting
Anaheim, California, November 8–13, 1992

NASA

These examples show that the method is applicable to higher frequency ranges.

NOMENCLATURE

A	total dimensionless area of finite element domain
$A^{(e)}$	area of element e
A_m^+	modal amplitude of wave moving in $+r$ direction away from origin
A_m^-	modal amplitude of wave moving in $-r$ direction towards origin
a	dimensionless circular cylinder radius $a^\#/L^\#$
$a^\#$	dimensional radius of circular cylinder (see superscripts)
$c^\#$	adiabatic speed of sound
e_r	error, Eq. (26)
F	column vector, right hand side of global matrix equation
f	dimensionless frequency, Eq. (2)
$H_m^{(1)}$	Hankel function of the first kind
$H_m^{(2)}$	Hankel function of the second kind
i	$\sqrt{-1}$
J_m	Bessel function of the first kind
K	global matrix, Eq. (23)
k	wave number, Eq. (4)
$L^\#$	characteristic distance
M	number of elements in finite element domain
M_c	number of modes needed for convergence to error e_r
M_{coef}	number of modal coefficients used in eigenfunction expansion
M_{pts}	number of grid points on interface S used in integration
m	mode number
m^*	mode number, Eq. (10)
N	number of nodes in finite element domain
$N^{(e)}$	local linear triangular interpolation function, $N^{(e)}(x,y)$ $N_i^{(e)}(x_j,y_j) = \delta_{i,j}$ ($i = 1,2,3$; $j = 1,2,3$)
N_S	number of grid points on interface S
n	normal vector
$\bar{n}$	outward unit normal vector
P	dimensionless perturbation acoustic pressure, $P^\#(x,y,t)/\rho_{o,ref}{}^\# c_{ref}{}^{\#2}$
p	dimensionless perturbation acoustic pressure $p(x,y) = P(x,y,t)/e^{-i\omega t}$
R_i	global residual error at node i
r	dimensionless radial coordinate
S	line interface between finite element and homogeneous domains
S_n	partial sum of series with n terms
S^+	region exterior to S
S^-	region interior to S
s	arc length parameter on S
t	dimensionless time, $t^\# c_{ref}{}^\#/L^\#$
W_i	global weight function associated with node i; $W_i(x_j,y_j) = \delta_{ij}$ ($i = 1 \ldots N$; $j = 1 \ldots N$)
$W_i^{(e)}$	local weight function associated with node i
W_{m^*}	interface weight function, Eq. (10)
x	dimensionless axial distance, $x^\#/L^\#$
y	dimensionless transverse distance, $y^\#/L^\#$
β	angle between element outward normal and x axis
δ_{ij}	Kronecker delta ($\delta_{ij} = 1$ for $i = j$; $\delta_{ij} = 0$ for $i \neq j$)
ϵ	dimensionless complex acoustic permittivity
θ	angle between radius vector and x axis
μ	dimensionless complex acoustic permeability
ρ	dimensionless perturbation (acoustic) density $\rho(x,y) = \rho^\#/\rho_{o,ref}{}^\#$
ρ_o	dimensionless ambient density, $\rho_o{}^\#(x,y)/\rho_{o,ref}{}^\#$ ($\rho_o(x,y) = 1$ for uniform properties)
ϕ	column solution vector, Eqs. (23) and (24)
$\omega^\#$	angular velocity, $2\pi f^\#$
ω	dimensionless angular velocity, Eq. (2)

Subscripts:

a	analytical solution
I	node location on interface S
i	node location in finite element domain
o	mean fluid condition
ref	arbitrary reference location for normalizing material properties
x	x component
y	y component

Superscripts:

$\sim$	approximate solution
$\#$	dimensional quantity
$'$	derivative with respect to argument
$\overline{(\ )}$	average value
(e)	element value
i	incident component
S	scattered component

METHOD OF ANALYSIS

The present study is concerned with computing the acoustic scattering by a symmetric two-dimensional body of an impinging plane wave traveling in the $+x$ direction. The spatial domain is divided into two subdomains, the homogeneous domain and the finite element domain, as shown in Fig. 1. The finite element domain contains a nodal grid system that covers the region of complicated geometry and material property variations. Linear triangular elements are used and the subdomain interface is approximated by piecewise linear segments. In the finite element domain, an approximate solution for the total (incident + scattered) acoustic pressure p is calculated by the Galerkin method. In the homogeneous domain, which extends to infinity, an analytic solution (an eigenfunction

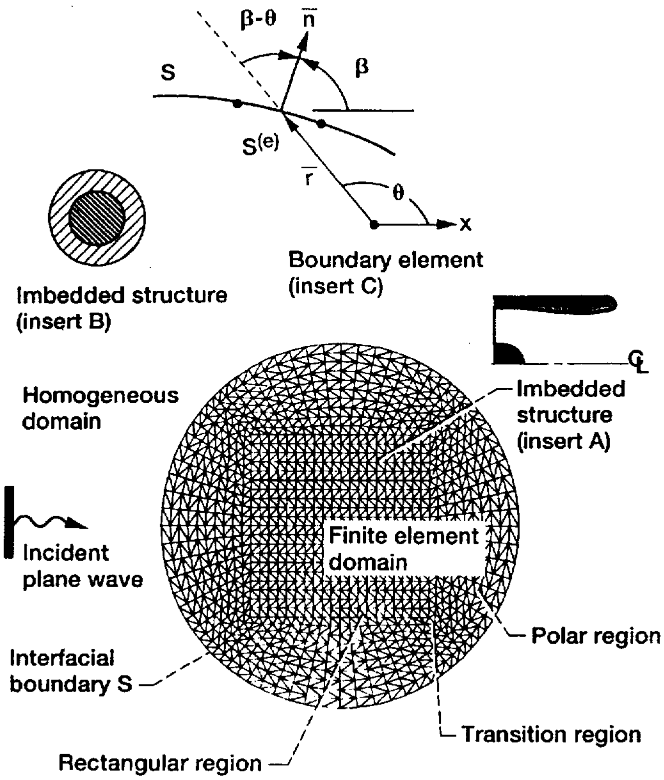

Figure 1.—Finite element grid system.

expansion) for the total acoustic pressure p_a is derived by separation of variables.

The modal element method couples the two solutions by imposing continuity on the pressure and velocity at the interface between the two subdomains. This coupling results in a single matrix equation in which the eigenfunction coefficients and the pressure at the finite element nodes are calculated simultaneously, yielding a global representation of the acoustic field. Generally, however, the desired quantity is the pressure field in the homogeneous domain, so the main goal is to find the eigenfunction coefficients; the finite element solution acts simply as a tool to obtain those coefficients.

GEOMETRICAL MODEL

A general finite element grid (Fig. 1) has been developed to study acoustic scattering from symmetric two-dimensional bodies with either hard (reflecting, rigid) or soft (absorbing) internal structures. The grid divides the finite element domain into rectangular, transition, and polar regions. The interior rectangular grid is used to model complicated geometries by a set of stepwise curve-fitting parameters, exemplified by Insert A (an aircraft inlet nacelle) in Fig. 1. The outer polar region is used to model more circular structures, such as an absorber-coated hull, as shown in Insert B in Fig. 1. The transition region links the polar and rectangular grid regions. The finite element domain can be restricted to the scattering body, or can extend as far beyond the body as desired.

For absorbing bodies, the entire body is covered with finite elements to track the propagation of an incident wave penetrating it. It is generally accepted that 12 nodes per wavelength are required when using linear elements, so the higher the frequency of the incident wave, the finer the grid must be.

For rigid bodies with simple shapes, it is possible to reduce the finite element structure inside the body to a single ring of elements following the body's contour, as shown in Fig. 2. This variation, the modal ring method, significantly reduces computation time and array sizes by eliminating nodes inside the body where the field does not penetrate. Coated rigid bodies could employ a small number of rings to calculate the pressure field in the penetrable coating.

GOVERNING EQUATIONS

Acoustic propagation in two-dimensional space can be modeled by the continuity, momentum, and state linearized gas dynamic equations in the absence of flow. For harmonic pressure propagation in a heterogeneous bulk material, Baumeister and Dahl (1987) used these equations to derive the following dimensionless wave equation:

$$\frac{\partial}{\partial x}\left(\frac{1}{\varepsilon}\frac{\partial p}{\partial x}\right) + \frac{\partial}{\partial y}\left(\frac{1}{\varepsilon}\frac{\partial p}{\partial y}\right) + \omega^2 \mu p = 0 \ , \tag{1}$$

where the dimensionless frequency associated with this Helmholtz-like equation is defined as:

$$f = \frac{L^{\#} f^{\#}}{c_{ref}{}^{\#}} \ , \qquad \omega = 2\pi f \ . \tag{2}$$

The notation is explicitly defined in the nomenclature. The reference location is arbitrarily chosen; all nondimensional properties are normalized to their reference values.

The relationship among acoustic "permittivity" ε, acoustic "permeability" μ, and the physical properties of the medium is complicated in the general case. However, for propagation in homogeneous media without dissipation, such as air, ε is the nondimensional ambient bulk fluid density and μ is its inverse:

$$\varepsilon = \rho_o(x,y) \ , \qquad \mu = \frac{1}{\rho_o(x,y)} \ . \tag{3}$$

For bulk absorbers, Baumeister and Dahl (1987, Eqs. (25) to (27)) employed Hersh's model (1980) in explicitly relating ε and μ to the porosity, a viscous loss coefficient, a heat transfer parameter, and an effective speed of sound of the medium. Briefly, for bulk absorbers, the real part of ε is related to ambient bulk fluid density while its imaginary part is proportional to a viscous loss coefficient. The μ

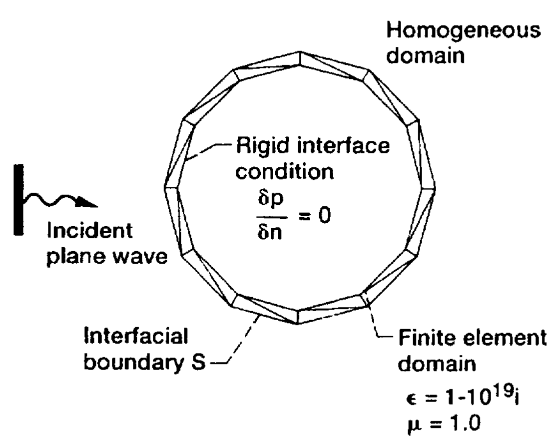

Figure 2.—Finite element ring grid system for rigid bodies.

term is inversely proportional to ambient bulk fluid density and the effective speed of sound, which depends on the heat transfer characteristics of the medium. The formulas for ε and μ are given by Baumeister and Dahl (1987, Eqs. (5) and (7)). Morse and Ingard (1986, p. 253) also developed more general parameters for describing propagation in porous media for which ε and μ can be related. For elastomeric materials, such as rubber, ε and μ are generally complex because of the complex nature of the propagation speed in the medium (Capps, 1989, p. 10). In the present paper, the parameters ε and μ are treated as mathematical quantities independent of property correlations. Both quantities are complex with the imaginary parts associated with dissipative losses.

In the homogeneous domain, the properties ε and μ are assumed constant. Thus, by substituting Eq. (3) into Eq. (2), the governing equation simplifies to

$$\frac{\partial^2 p_a}{\partial x^2} + \frac{\partial^2 p_a}{\partial y^2} + k^2\, p_a = 0, \tag{4}$$

where $k^2 = \omega^2 \mu \varepsilon$. The subscript a is introduced to indicate that the acoustic pressure solution designated by p_a is the analytical solution that applies in the homogeneous domain, in contrast to the pressure p designating the pressure in the finite element domain.

ANALYTIC SOLUTION

In the homogeneous domain, an exact eigenfunction expansion can be derived from Eq. (4) by separation of variables. This expansion, valid only in the homogeneous domain, is linked to the finite element solution, valid only in the finite element domain, by the modal element method.

Consider an acoustic pressure plane wave traveling in the +x direction, striking a symmetric two-dimensional scatterer. In the homogeneous domain, the expression for the total pressure p_a can be broken into the incident plane wave and the scattered wave:

$$p_a = p_a^i + p_a^s , \tag{5}$$

where p_a^i is the incident wave and p_a^s is the scattered wave. A plane wave moving in the +x direction has the form

$$p_a^i = e^{ikx} = e^{ikr\cos(\theta)} = J_o(kr) + 2 \sum_{m=1}^{\infty} i^m \cos(m\theta) J_m(kr) , \tag{6}$$

when the time dependence is assumed to be $e^{-i\omega t}$.

The eigenfunction expansion in two dimensions is written in the following form (Morse and Ingard, 1968, p. 401):

$$p_a = \sum_{m=0}^{M_{coef}-1} A_m^+ H_m^{(1)}(kr)\cos(m\theta) + A_m^- H_m^{(2)}(kr)\cos(m\theta) . \tag{7}$$

Equation (7) is valid only for problems that are symmetric with respect to the x-axis because of the assumed mathematical form of the incident wave in Eq. (6) (Eq. 1.2.9 Morse and Ingard) which leads to the cosine term in Eq. (7). Due to the form of the time dependence, $H_m^{(1)}$ terms correspond to waves traveling outward in the +r direction and $H_m^{(2)}$ terms correspond to inward traveling waves. The scattered wave is then written as

$$p_a^s = \sum_{m=0}^{M_{coef}-1} A_m^+ H_m^{(1)}(kr)\cos(m\theta) , \tag{8}$$

where M_{coef}, the number of coefficients used in the expansion, must be set a priori. Hereafter, the eigenfunction terms are called modes, as commonly used in acoustic theory. Equation (8) satisfies the far field boundary condition—scattered waves move outwardly. The coefficients A_m^+ are unknown, to be determined by the imposition of interface conditions.

INTERFACE CONDITIONS

At the interface S between the finite element domain and the homogeneous domain, both pressure and velocity are continuous (Temkin, 1981, p. 80). The continuity of pressure

$$p|_{S^+} - p|_{S^-} = 0 \tag{9}$$

can be expressed numerically by a collocation procedure (Lee and Cendes, 1987) or an integral weighting procedure (Baumeister, 1986b, Eq. (45)). The latter is used here with weight functions $\cos(m^* \Theta)$, so the continuity of pressure at the interface is expressed by

$$\oint_{S,\ \theta=0}^{\theta=2\pi} W_{m^*} \left[p_a - p\right] ds = 0 . \qquad W_{m^*} = \cos(m^* \theta) \qquad (m^* = 0,1,2,\ldots,M_{coef}-1 \ \text{ equations}) \tag{10}$$

In general, S can be parameterized by a function of r and θ, introducing a θ dependence into ds. Unless S is a circle, then, the orthogonality of the cosine functions cannot be used, and a completely numerical approach must be adopted to determine equations for the A_m^+.

For the problems considered so far, it suffices to apply a simple quadrature to obtain acceptable results when approximating Eq. (10). S is divided into subintervals centered at points (r_I, θ_I), which correspond to finite element nodes introduced later in the paper. Once M_{coef} has been determined (based on the incident wave frequency and data in Figs. 3 and 4), the grid is set up so that the number of nodes on S is $N_S \geq 12 M_{coef}$ to adequately resolve the pressure field. Experimentation has determined that, at least for simple geometries, not all of these points need to be used in the quadrature to approximate Eq. (10) accurately. In the examples presented later, the number of points used is $M_{pts} = 2M_{coef}$. These nodes are equally spaced around a circular interface S, so every sixth point is used in the quadrature below.

It is highly desirable to reduce the number of nodes used; doing so reduces the bandwidth of the solution matrix and yields a large savings in core storage and computation time. For more complicated problems, however, it will probably be necessary to use a better quadrature to approximate Eq. (10), which may increase computing requirements.

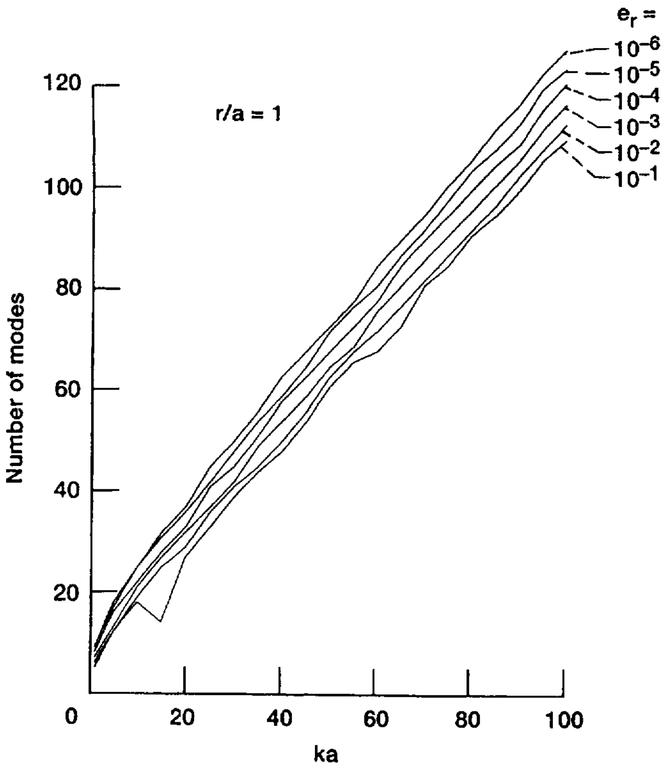

Figure 3.—Number of modes required to resolve the scattered acoustic pressure field on a cylinder of radius a subjected to a plane wave impingement for a relative error e_r.

Applying the midpoint rule to the chosen nodes gives

$$\sum_{I=1}^{M_{pts}}{}_S \; [p_a(r_I,\theta_I) - p_I]\cos(m^*\theta_I) r_I \, \Delta\theta_I = 0 \; . \tag{11}$$

$$(m^* = 0,1,2,\ldots,M_{coef}-1 \quad \text{equations})$$

By expressing p_a in terms of the modal coefficients in Eq. (8), Eq. (11) can be written explicitly as

$$\sum_{I=1}^{M_{pts}}{}_S \; r_I \, \Delta\theta_I \cos(m^*\theta_I)$$

$$\times \left[e^{ikr_I \cos\theta_I} + \sum_{m=0}^{M_{coef}-1} A_m^+ H_m^{(1)}(kr_I)\cos(m\theta_I) - p_I \right] = 0 \; . \tag{12}$$

$$(m^* = 0,1,2,\ldots,M_{coef}-1 \quad \text{equations})$$

Equation (12) comprises M_{coef} separate difference equations, each of which is written in terms of all the unknown coefficients A_m^+ and the pressure p_I at the nodes on S. These equations are combined with the finite element equations presented below to form a matrix system which yields all the unknowns at once.

The continuity of velocity (Baumeister and Dahl, 1987, Eq. (21)) requires that at the interface

$$\frac{1}{\epsilon_a}\frac{\partial p_a}{\partial n}\bigg|_{S^+} = \frac{1}{\epsilon}\frac{\partial p}{\partial n}\bigg|_{S^-} \; , \tag{13}$$

where n is the outward normal. This relationship is key to the modal element method, as indicated below.

BOUNDARY CONDITIONS

The pressure field is scaled appropriately by introducing the normalized incident wave in Eq. (6). The far field radiation boundary condition is satisfied exactly by the assumed form of p_a^s in Eq. (8). The pressure continuity across the domain interface is enforced by Eq. (12), and the velocity continuity across the interface by Eq. (13). No special handling of acoustic boundary conditions at media interfaces within the finite element region is required because the variable property form of the wave equation has been employed. Any change in internal structure in the finite element region can be simulated merely by changing the properties of the elements in the finite element domain, as shown by Baumeister and Dahl (1989).

FINITE ELEMENT SOLUTION

The finite element domain, with total area A, is divided into M discrete triangular elements, $A^{(e)}$, e = 1,2,...,M, defined by N corner nodal points (x_i,y_i), i = ,2,...,N. The corner nodes for area $A^{(e)}$ are denoted $[x_1^{(e)},y_1^{(e)}]$, $[x_2^{(e)},y_2^{(e)}]$, and $[x_3^{(e)},y_3^{(e)}]$. It is assumed that all material properties are constant in each element.

The acoustic pressure is approximated by a linear combination of weight functions $W_i(x,y)$:

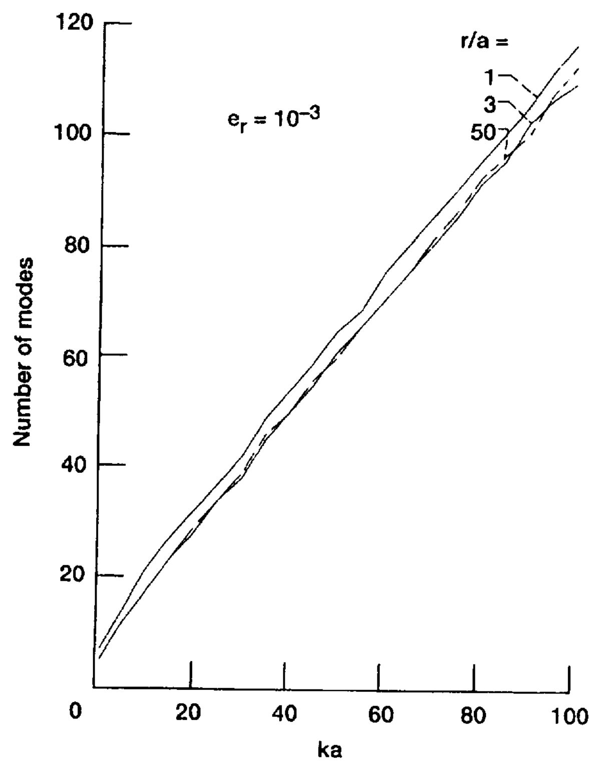

Figure 4.—Number of modes required to resolve the scattered acoustic pressure field around a cylinder of radius a subjected to a plane wave impingement, at various radii, for relative error $e_r = 10^{-3}$.

$$\tilde{p}(x,y) = \sum_{i=1}^{N} W_i(x,y)p_i = [W(x,y)]\{p\} , \tag{14}$$

with [ ] representing a row vector and { } representing a column vector. The weights have the property that

$$W_i(x_j,y_j) = \delta_{ij} \qquad \text{(Kronecker delta)} , \tag{15}$$

so that the unknown nodal pressure values are given by $p_i = \tilde{p}\,(x_i,y_i)$.

To determine $\{p\}$, apply the method of weighted residuals. In this method, the residual error of Eq. (1),

$$R_i = \int\int_A W_i \left(\nabla \cdot \frac{1}{\varepsilon}\nabla\tilde{p} + \omega^2\mu\tilde{p}\right) dx\,dy \tag{16}$$

$$(i = 1,2,3,...N \quad \text{one residual equation for each node } i)$$

is set to 0 for each node i. Applying the divergence theorem to the first term of the integrand in Eq. (16) yields the weak formulation of Eq. (1):

$$R_i = \int\int_A \left(\nabla W_i \cdot \frac{1}{\varepsilon}\nabla\tilde{p} + W_i\omega^2\mu\tilde{p}\right) dx\,dy - \int_S \left(W_i\frac{1}{\varepsilon}\nabla\tilde{p} \cdot \bar{n}\right) ds = 0 .$$

$$(i = 1,2,3,...N \quad \text{one global finite difference equation for each node } i) \tag{17}$$

Equation (17) is a global, or node-oriented, formulation, in that it provides a difference equation for each node that can be used to determine $\{p\}$.

From a practical standpoint, though, it is more convenient to consider a local, or element-oriented, formulation, which more easily provides the same difference equation for each node. To develop the local formulation, write each residual R_i as the sum of the element residuals:

$$0 = R_i = \sum_{e=1}^{M} R_i^{(e)} = \sum_{e=1}^{M} \left[\int\int_{A^{(e)}} \left(\nabla W_i^{(e)} \cdot \frac{1}{\varepsilon}\nabla\tilde{p}^{(e)} + W_i^{(e)}\omega^2\mu\tilde{p}^{(e)}\right) dA - \int_{S^{(e)}\cap S} \left(W_i^{(e)}\frac{1}{\varepsilon}\nabla\tilde{p}^{(e)} \cdot \bar{n}\right) ds \right] ,$$

$$(i = 1,2,3,...N \quad \text{one global finite difference equation for each node } i) \tag{18}$$

where $S^{(e)}$ is the boundary of element $A^{(e)}$. Note that for standard weight functions, the line integral in Eq. (18) vanishes unless node i is on the boundary S.

In order to evaluate the integrals in Eq. (18), it is necessary to represent $\tilde{p}\,(x,y)$ locally. Let $N_j^{(e)}$, $j = 1,2,3$, be the local linear shape functions associated with each corner node (Segerlind, 1976, p. 29), so that

$$\tilde{p}^{(e)}(x,y) = N_1^{(e)}(x,y)p_1^{(e)} + N_2^{(e)}(x,y)p_2^{(e)} + N_3^{(e)}(x,y)p_3^{(e)} = \sum_{j=1}^{3} N_j^{(e)}(x,y)p_j^{(e)} = [N^{(e)}(x,y)]\{p^{(e)}\} . \tag{19}$$

Now implement the Galerkin method—let the local weight function $W_i^{(e)}$ associated with node $(x_i^{(e)},y_i^{(e)})$ equal $N_i^{(e)}$. The global shape function W_i is identically zero for any element where node i does not appear.

In the boundary integral terms in Eq. (18), it is reasonable to approximate the (continuous) normal derivative with its mean value over $S^{(e)}\cap S$. The key step is to apply the continuity of velocity (Eq. (13)), which introduces the eigenfunction coefficients, thus linking the analytic solution and the finite element solution on the interface. The term is transformed as follows:

$$\begin{aligned}\int_{S^{(e)}\cap S} \left(W_i^{(e)}\frac{1}{\varepsilon}\nabla\tilde{p}^{(e)} \cdot \bar{n}\right) ds &= \int_{S^{(e)}\cap S} \left(N_i^{(e)}\frac{1}{\varepsilon}\frac{\partial\tilde{p}^{(e)}}{\partial n}\right) ds \\ &= \overline{\frac{1}{\varepsilon_a}\left(\frac{\partial p_a}{\partial n}\right)_{S^{(e)}}} \int_{S^{(e)}\cap S} N_i^{(e)} ds \\ &= \overline{\frac{1}{\varepsilon_a}\left(\frac{\partial p_a}{\partial r}\cos(\beta-\theta) + \frac{1}{r}\frac{\partial p_a}{\partial \theta}\sin(\beta-\theta)\right)_{S^{(e)}}} \int_{S^{(e)}\cap S} N_i^{(e)} ds ,\end{aligned} \tag{20}$$

where ß and θ are shown in the insert in Fig. 1.

Substituting Eqs. (19) and (20) into Eq. (18) and employing the Galerkin approximation yield

$$0 = R_i = \sum_{e=1}^{M} \left[\int\int_{A^{(e)}} \left(\frac{1}{\varepsilon^{(e)}}\nabla N_i^{(e)} \cdot \nabla[N^{(e)}] - \omega^2\mu^{(e)}N_i^{(e)}[N^{(e)}]\right)\{p^{(e)}\}\, dA - \overline{\frac{1}{\varepsilon_a}\left(\frac{\partial p_a}{\partial r}\cos(\beta-\theta) + \frac{1}{r}\frac{\partial p_a}{\partial \theta}\sin(\beta-\theta)\right)_{S^{(e)}}} \int_{S^{(e)}\cap S} N_i^{(e)} ds \right] .$$

$$(i = 1,2,3,...N \quad \text{one global finite difference equation for each node } i) \tag{21}$$

For each value of i, Eq. (21) can be evaluated explicitly using the standard definition of $N_i(x,y)$ for linear triangular elements (Segerlind, 1976, p. 29).

Combining Eqs. (21) and (12) provides the final form of the matrix equation

$$K\,\{\phi\} = \{F\}, \tag{22}$$

where

$$\{\phi\}^T = \left[A_1^+,A_2^+,...,A_{M_{coef}}^+,p_1,p_2,...,p_N\right] . \tag{23}$$

F contains the incident plane wave terms present in Eq. (12) and in the derivatives of p_a in Eq. (21). The matrix K has the following general form

$$\left[\begin{array}{c|c} A^{(12)} & P^{(12)} \\ \hline A^{(22)} & P^{(22)} \end{array}\right]$$

The submatrix $A^{(12)}$ is a full $M_{coef} \times M_{coef}$ matrix composed of the coefficients of the A_m^+ terms in Eq. (12). The submatrix $P^{(12)}$ is a sparse $M_{coef} \times N$ matrix composed of the coefficients of p_I in Eq. (12). $A^{(22)}$ is an $N \times M_{coef}$ matrix composed of the coefficients of A_m^+ from the surface integral in Eq. (21). For each boundary node, there is a full row of terms in $A^{(22)}$, with a full row of zeros for interior nodes. $P^{(22)}$ is a sparse, highly banded $N \times N$ matrix composed of the coefficients of p_I in Eq. (21).

Equation (22) is solved by a frontal solver. The number of columns kept in core is roughly $M_{coef} + M_{pts}/2$ + bandwidth of $P^{(22)}$.

RESULTS AND COMPARISONS

In order to validate the method, several numerical experiments are presented. First, a description of the number of modes required for convergence in Eq. (8) is given, and a simple formula is provided. Example 1 shows the simple case of a plane wave passing through air. Examples 2 and 3 describe the problem of scattering from a hard rigid cylinder, using the modal element method and the modal ring method, respectively. Both numerical results agree closely with the exact solution for these problems. Finally, scattering from a hard circular cylinder with an absorbent coating is presented in Example 4. These examples give an indication of the value of the modal element method: the speed and accuracy of the calculations, the relatively low matrix storage costs, the wide frequency range available, and the flexibility to handle problems of complicated geometry and material property variation.

For the circular cylinder examples to follow, the characteristic length $L^{\#}$ is set equal to the radius of the circular cylinder. Consequently, the dimensionless radius $a = 1$ in all examples.

It is of practical interest to determine the number of modes necessary for the series in Eq. (8) to converge. As more modes are needed, more finite element nodes on the interface are also needed, and hence more computing resources are required. To get a rough idea of the number of modes needed for a particular application, consider the expression for the scattered field generated by an incident plane wave (as in Eq. (6)) striking a hard cylinder. This expression is given by the infinite series associated with Eq. (8), where (Bowman et al., Eq. (2.38))

$$A_m^+ = \frac{-(2 - \delta_{m0})\, i^m J_m'(ka)}{H_m^{(1)'}(ka)} . \tag{24}$$

Clearly, the number of modes is determined by ka, the observation radius r, and the desired accuracy of the solution. For the data presented in Figs. 3 and 4, accuracy is measured relatively; that is, letting the partial sums of the series be denoted by S_n, the series has converged if

$$\frac{(S_{n+1} - S_n)}{S_n} \le e_r . \tag{25}$$

In Fig. 3, the number of modes needed for various e_r values is compared with ka, on the surface of the cylinder ($r = a$). The data clearly shows that as e_r decreases, the number of required modes increases, as expected. However, the increase is slow enough that only a few extra terms are needed to improve the accuracy significantly. For example, if $ka = 100$, then 110 modes are required for $e_r = 10^{-1}$, but only 18 more modes are needed to improve the accuracy to $e_r = 10^{-6}$. Similar results hold off the surface, in both the near and far fields. Note that for the most computationally intensive case considered ($ka = 100$, $e_r = 10^{-6}$), the number of columns kept in core by the frontal solver is under 300.

It might be expected that the number of required modes increases in the far field, but Fig. 4 indicates otherwise. As r increases, the amplitude of $H_m^{(1)}$ decreases, so the terms are smaller and the series converges faster. As seen in the figure, the decrease in the number of terms is slight, and occurs even for small r/a values. The data in Fig. 4 is for $e_r = 10^{-3}$, but is representative of all the other e_r values.

The following formulas give a rough indication of the number of modes needed for convergence:

$$M_c = \text{int}\left(\left[7 + \log_{10}\left(\frac{1}{\epsilon}\right)\right] + \left[1.16 + 0.04\log_{10}\left(\frac{1}{\epsilon}\right)\right](ka)\right) \tag{26}$$

$$ka \le 15 ,$$

$$M_c = \text{int}\left(\left[10 + \log_{10}\left(\frac{1}{\epsilon}\right)\right] + \left[1.00 + 0.03\log_{10}\left(\frac{1}{\epsilon}\right)\right](ka)\right) \tag{27}$$

$$ka > 15 .$$

Equation (27) is valid for ka up to 100, and may be accurate for larger ka values. In many cases, the number of terms indicated by the formulas is slightly larger than the number of terms actually needed, but is nowhere smaller. The worst observed difference is for $ka = 100$, $e_r = 10^{-6}$, where 128 terms are required, but the formula gives 134. The equations are valid on the surface as well as in the far field.

Figures 3 and 4 are not valid for a general problem. However, they represent a good starting point for estimating the number of modes required for convergence.

In each of the following examples, a unit plane wave, incident from the left, strikes a cylinder oriented with its axis normal to the propagation direction.

Example 1. - Propagation Through Air

Consider the incident plane wave propagating through air and impinging on an imaginary cylinder (radius 1) composed of air. The modal element method verifies that there is no reflection from the cylinder and the pressure amplitude inside and outside the cylinder is 1. Figure 5 shows the pressure amplitude at the interface between the finite element and homogeneous domains. For a relatively coarse grid, the first few calculated modal coefficients (which should vanish) are:

$$A_0^+ = -0.33424\times10^{-4} - 0.57905\times10^{-2}\, i$$
$$A_1^+ = -0.13103\times10^{-2} - 0.18505\times10^{-4}\, i$$
$$A_2^+ = 0.12062\times10^{-5} + 0.45241\times10^{-3}\, i$$

Example 2. - Rigid Cylinder, Modal Element Method

Consider the incident plane wave striking a solid rigid cylinder of dimensionless radius $r = 1$, with $ka = 1$. For all internal elements, the permittivity is set to $\epsilon = 1 - 10^{19}\, i$ to approximate a hard cylinder. The finite element domain extends to $r = 1.5$; in this case the polar region contains air, although it could be filled with an absorbing material, as in Example 4.

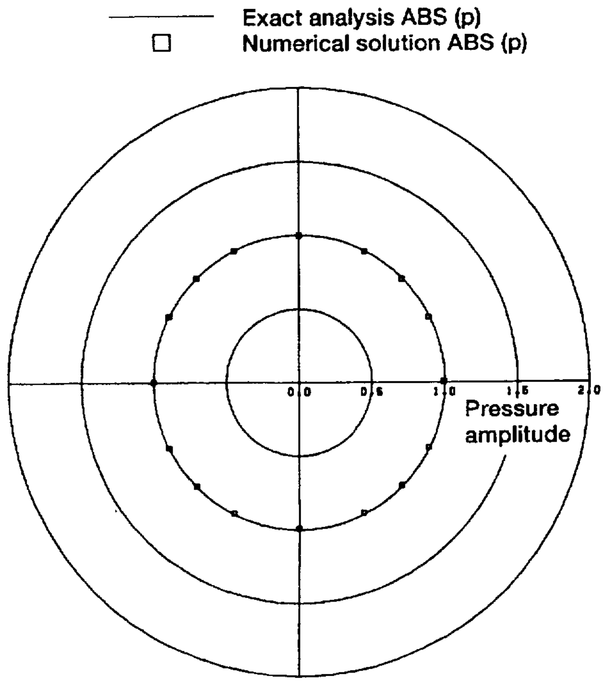

Figure 5.—Polar plot of the total acoustic pressure around a cylinder composed of air (zero scattering, k = 0.628, r = 1.0, 57 nodes, 96 elements, Δx = Δy = 0.25 in rectangular region), interface at r = 1.

In Fig. 6, the pressure amplitude is plotted against azimuthal angle for ka = 1. Figure 6(a) shows the pressure on the cylinder's surface (r = 1), while Fig. 6(b) shows the pressure at r = 1.5. Since these radii are both in the finite element domain, the finite element solutions (hollow boxes) are compared to the exact solution (solid line). Clearly, the method gives excellent results.

In Fig. 7, the pressure amplitude is plotted again for ka = 1, but for larger radii in the homogeneous domain. In these plots, the numerical solution is generated from the calculated modal coefficients A_m^+ using Eqs. (5), (6), and (8). Plots for r = 1.5 (7a), r = 3.18 (7b), r = 7.95 (7c), and r = 15.9 (7d) are shown. Again, there is excellent agreement between the numerical solutions (hollow boxes) and exact solutions (solid lines).

The grid shown in Fig. 1 was used to generate the data presented in Figs. 6 and 7. Recall that from the analysis summarized in Fig. 4, if a given set of modes accurately describes the pressure field on the surface of the solid cylinder, then the pressure is accurately described for all larger radii, since the required number of modes decreases in the far field. The first few calculated modal coefficients are:

Numerical Solution	Exact Solution
$A_0^+ = -0.23066E{-}00 - 0.42154E{-}00i$	$A_0^+ = -0.24087E{-}00 - 0.42761E{-}00i$
$A_1^+ = -0.67095E{-}00 - 0.25833E{-}00i$	$A_1^+ = -0.65615E{-}00 - 0.24537E{-}00i$
$A_2^+ = +0.14075E{-}01 - 0.16638E{-}00i$	$A_2^+ = +0.13823E{-}01 - 0.16569E{-}00i$
$A_3^+ = +0.70539E{-}02 + 0.11636E{-}03i$	$A_3^+ = +0.71092E{-}02 + 0.25271E{-}04i$
$A_4^+ = -0.49985E{-}06 + 0.13701E{-}03i$	$A_4^+ = -0.11510E{-}07 + 0.15172E{-}03i$
$A_5^+ = -0.66943E{-}05 - 0.45628E{-}06i$	$A_5^+ = -0.19355E{-}05 - 0.18731E{-}11i$
$A_6^+ = +0.13118E{-}07 - 0.21266E{-}06i$	$A_6^+ = +0.13400E{-}15 - 0.16371E{-}07i$
$A_7^+ = -0.55536E{-}07 - 0.29859E{-}07i$	$A_7^+ = +0.98529E{-}10 + 0.48540E{-}20i$
$A_8^+ = +0.22121E{-}09 - 0.70338E{-}09i$	$A_8^+ = -0.98392E{-}25 + 0.44360E{-}12i$

Clearly, the numerical and exact values of the modes are very close for those modes which make a significant contribution to the scattered field.

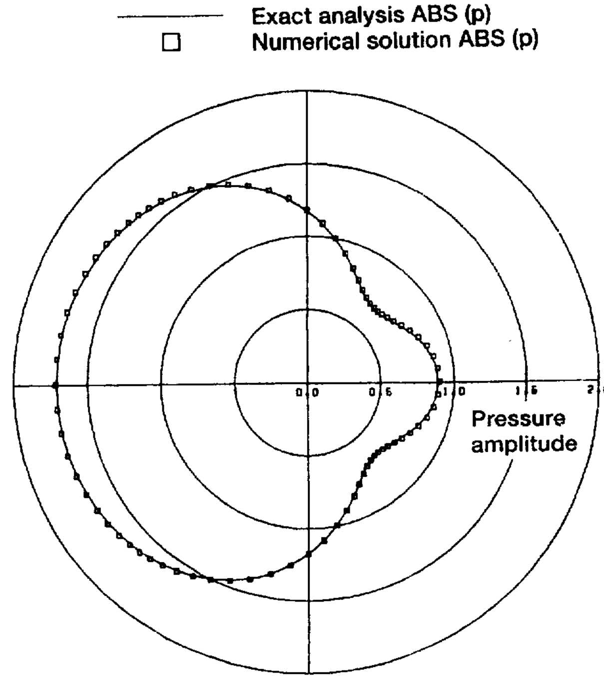

(a) r = 1.0.

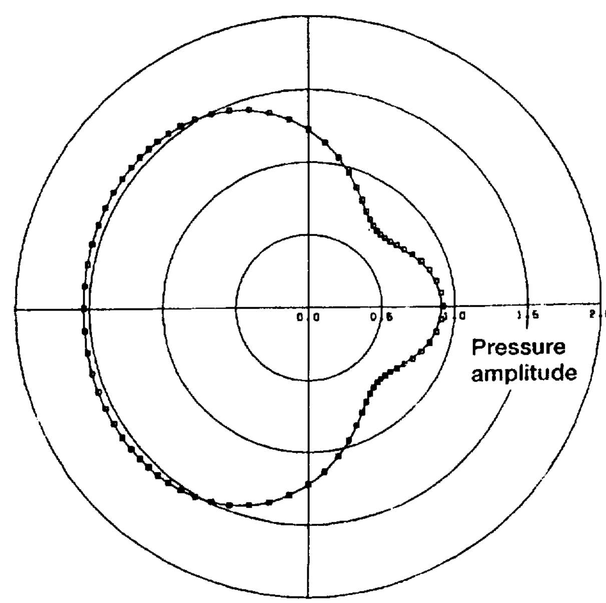

(b) r = 1.5.

Figure 6.—Polar plot of the total acoustic pressure at node points around a solid cylinder subjected to a plane wave impingement (k = 1.0, a = 1.0, 1865 nodes, 3648 elements, Δx = Δy = 0.05 in rectangular region), interface at r = 1.5.

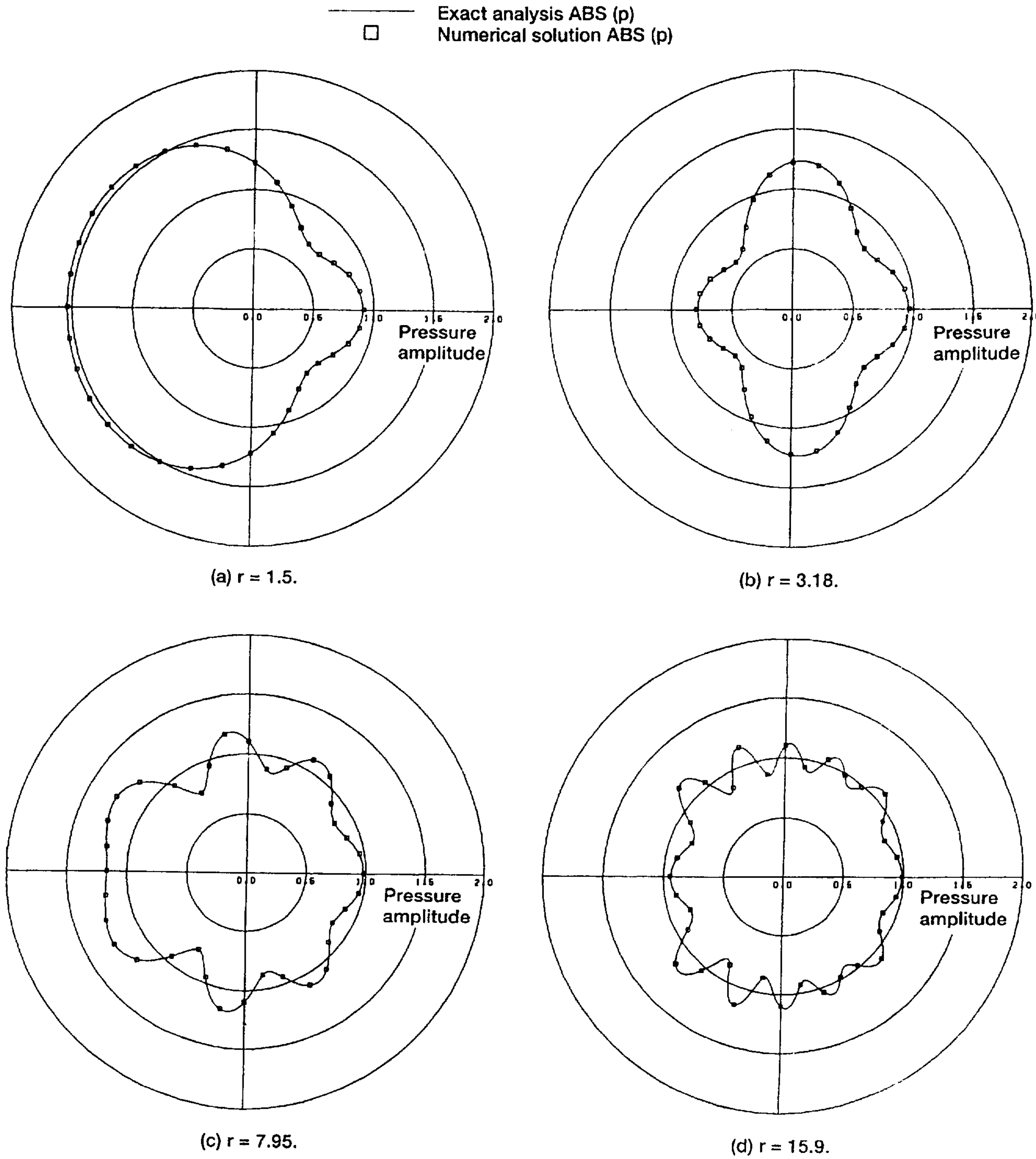

Figure 7.—Polar plot of the total acoustic pressure around a solid cylinder subjected to a plane wave impingement reconstructed from modal-element method modal coefficients ($k = 1.0$, $a = 1.0$, 1865 nodes, 3648 elements, $\Delta x = \Delta y = 0.05$ in rectangular region), interface at $r = 1.5$.

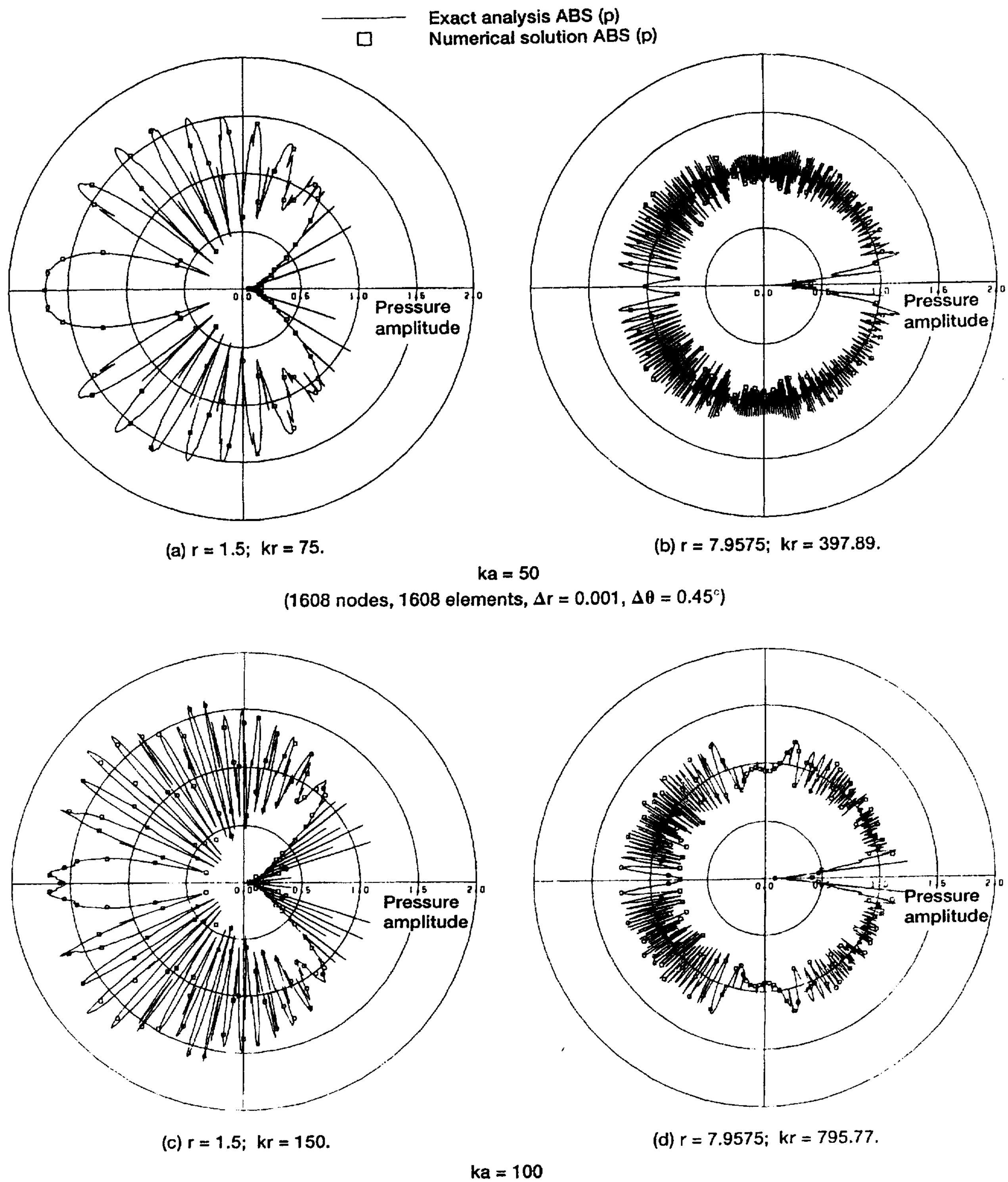

(a) r = 1.5; kr = 75.

(b) r = 7.9575; kr = 397.89.

ka = 50

(1608 nodes, 1608 elements, $\Delta r = 0.001$, $\Delta\theta = 0.45°$)

(c) r = 1.5; kr = 150.

(d) r = 7.9575; kr = 795.77.

ka = 100

(2904 nodes, 2904 elements, $\Delta r = 0.0005$, $\Delta\theta = 0.25°$)

Figure 8.—Polar plot of the total acoustic pressure around a solid cylinder subjected to a plane wave impingement constructed from modal coefficients determined by modal-ring method.

Example 3 - Rigid Cylinder, Modal Ring Method

Consider a high frequency incident plane wave striking a solid rigid cylinder of dimensionless radius r = 1. The modal ring method, using a grid similar to that of Fig. 2, is used to generate the pressure amplitude plots in Fig. 8 for frequencies corresponding to ka = 50 and ka = 100 at r = 1 and r = 7.9575. Choosing as an acceptable relative error $\epsilon = 10^{-3}$, the number of modes required to resolve the scattered field is $M_c = 67$ for ka = 50 (Figs. 8(a) and (b)) and $M_c = 121$ for ka = 100 (Figs. 8(c) and (d)). The total number of finite element nodes used is $24M_c$ ($12M_c$ each on the interface and the outer ring). The excellent agreement between the numerical solutions (hollow squares) and the exact solutions (solid lines) clearly indicates that the modal ring method is suitable for high frequency scattering applications.

As an additional consideration, when the modal ring method is applied to a low frequency scattering problem considered by Khan, Brown and Ahuja (their Fig. 3), the modal ring method gives more accurate results with a reduction of two orders of magnitude in the number of grid points.

Example 4. - Coated Rigid Cylinder

Consider the incident plane wave impinging on a cylinder of dimensionless radius r = 1 that has a rigid solid core of radius 0.9 and an absorbing coating of thickness 0.1. The solid rigid core is approximated by setting $\epsilon = 1 - 10^{19}\,i$ while the coating has $\epsilon = \mu = 1 - 5i$. The grid shown in Fig. 1 was used in this example. Figure 9 shows the calculated pressure amplitude at r = 3.18. The effect of the coating is apparent by comparing this figure with Fig. 7(b). The profiles have the same general shape but the coating induces slightly more backscatter ($\theta = 0$), and slightly less scattering at $\theta = 135, 225°$. Because the modal element method is relatively inexpensive to run, it could be used to identify coatings that maximize the absorption of acoustic energy.

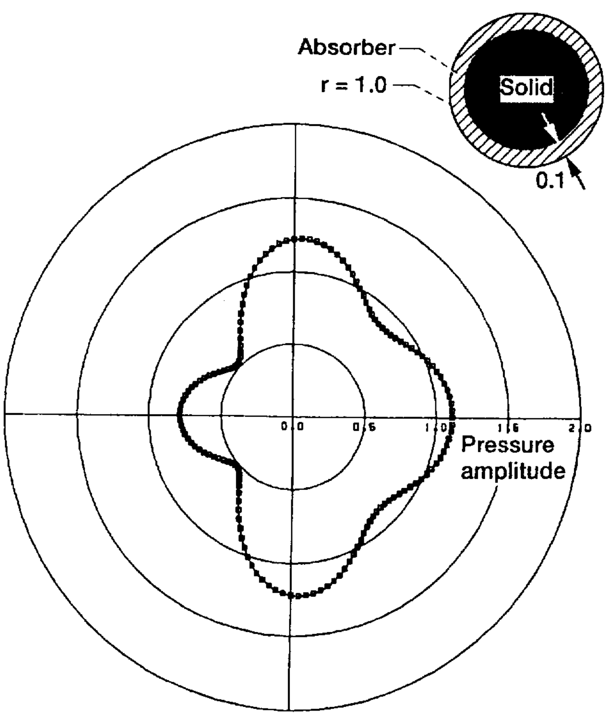

Figure 9.—Polar plot of the total acoustic pressure around a coated cylinder subjected to a plane wave impingement reconstructed from a modal-element method modal coefficients (k = 1.0, a = 1.0, r = 3.18, ϵ = 1-i5, μ = 1-i5, 1145 nodes, 2208 elements, $\Delta x = \Delta y = 0.05$ in rectangular region), interface at r = 1.

CONCLUDING REMARKS

The modal element method for acoustic scattering from a two-dimensional body is presented. The body may be acoustically hard (reflecting) or soft (absorbing). The acoustic pressure field is represented by a finite element solution in the bounded finite element domain containing the body, and by an exact eigenfunction expansion in the unbounded exterior homogeneous domain. The two representations are coupled by the continuity of pressure and velocity across the interface between the two subdomains, and are calculated simultaneously from a single matrix equation. The method is applicable to problems involving high or low frequency scattering.

The analysis for two-dimensional scattering from solid and coated bodies is presented, and several simple numerical examples are discussed. The examples are provided for validation—the numerical results show excellent agreement with the corresponding exact solutions. More detailed numerical work is planned.

For scattering from rigid bodies, the modal ring grid offers an attractive low storage approach to handling high frequency scattering. The modal ring grid effectively reduces the two-dimensional problem to a one-dimensional problem similar to the boundary element method. The ring grid offers the added advantage of being able to handle rigid bodies with coatings.

REFERENCES

Astley, R.J., and Eversman, W., 1981, "Acoustic Transmission in Non-Uniform Ducts with Mean Flow, Part II: The Finite Element Method," Journal of Sound and Vibration, Vol. 74, pp. 103-121.

Baumeister, K.J., 1980, "Time-Dependent Difference Theory for Noise Propagation in a Two-Dimensional Duct," AIAA Journal, Vol. 18, No. 12, pp. 1470-1476.

Baumeister, K.J., and Horowitz, S.J., 1984, "Finite Element-Integral Acoustic Simulation of JT15D Turbofan Engine," Journal of Vibration, Acoustics, Stress and Reliability in Design, Vol. 106, pp. 405-413.

Baumeister, K.J., 1986a, "Time-Dependent Wave Envelope Finite Difference Analysis of Sound Propagation," AIAA Journal, Vol. 24, No. 1, pp. 32-38.

Baumeister, K.J., 1986b, "Finite Element Analysis of Electromagnetic Propagation in an Absorbing Wave Guide," NASA TM-88866.

Baumeister, K.J., and Dahl, M.D., 1987, "A Finite Element Model for Wave Propagation in an Inhomogeneous Material Including Experimental Validation," AIAA Paper 87-2741 (also NASA TM-100149).

Baumeister, K.J., and Dahl, M.D., 1989, "Acoustic Wave Propagation in Heterogeneous Structures Including Experimental Validation," AIAA Paper 89-1044 (also NASA TM-101486).

Baumeister, K.J., Eversman, W., Astley, R.J., and White, J.W., 1983, "Acoustics in Variable Area Duct: Finite Element and Finite Difference Comparison to Experiment: AIAA Journal, Vol. 21, No 2, pp. 193-199.

Bowman, J.J., Senior, T.B.A., and Uslenghi, P.L.E., 1969, Electromagnetic and Acoustic Scattering by Simple Shapes, North-Holland Publishing Company, Amsterdam.

Capps, R.N., 1989, "Elastomeric Materials for Acoustical Applications," Naval Research Laboratory, Report 4311.

Chang, S.K., and Mei, K.K., 1976, "Application of the Unimoment Method to Electromagnetic Scattering of Dielectric Cylinders," IEEE Transaction on Antennas and Propagation, Vol. AP-24, No. 1, pp. 35-42.

Hersh, A.S., and Walker, B., 1980, "Acoustic Behavior of Fibrous Bulk Materials," AIAA Paper 80-0986.

Khan, M.M.S., Brown, W.H., and Ahuja, K.K., 1986, "Computational Aeroacoustics as Applied to the Diffraction of Sound by Cylindrical Bodies," AIAA Paper 86-1879.

Lee, J.-F., and Cendes, Z.J., 1987, "The Transfinite Element Method for Computing Electromagnetic Scattering From Arbitrary Lossy Cylinders," Paper AP03-5, AP-S International Symposium, New York, Vol. 1, pp. 99-102.

Ling, R.T., 1986, "Numerical Solution for the Scattering of Sound Waves by a Circular Cylinder," AIAA Paper 86-1880.

Ling, R.T., and Smith, T.D., 1988, "Scattering of Acoustic and Electromagnetic Waves by an Airfoil," AIAA Paper 88-0180.

Morse, P.M., and Ingard, K.U., 1968, "Theoretical Acoustics," McGraw-Hill, New York.

Segerlind, L.J., 1976, "Applied Finite Element Analysis," John Wiley & Sons, New York.

Seybert, A.F., and Soenarko, B., 1987, "Radiation and Scattering of Acoustic Waves from Bodies of Arbitrary Shape in a Three-Dimensional Half Space," Journal of Vibration, Acoustics, Stress, and Reliability in Design, Vol. 110, No. 1, pp. 112-117 (also ASME Paper 87-WA/NCA-14).

Taflove, A., Kriegsman, G.A., and Umashankar, K.R., 1986, "Advanced Numerical Modeling of Electromagnetic Wave Interactions with Complex, Electrically-Large Structures," Vol. 1, Short Course Notes, Northwestern University Technological Institute, Evanston, IL.

Temkin, S., 1981, "Elements of Acoustics," John Wiley and Sons, New York.

Umashanker, K.R., and Taflove, A., 1982, "A Novel Method to Analyze Electromagnetic Scattering of Complex Objects," IEEE Transactions on Electromagnetic Compatibility, Vol. EMC-24, pp. 397-405.

Umashanker, K.R., and Taflove, A., 1984, "Analytical Models for Electromagnetic Scattering," Final Report on IITRI Project E06538, Air Force Contract F19628-82-C-0140.

Watson, W., and Myers, M., 1990, "A Two-Step Iteractive Method for Evolving Nonlinear Acoustic Systems to a Steady-State," AIAA Paper 90-3946.

REPORT DOCUMENTATION PAGE

Form Approved
OMB No. 0704-0188

1. AGENCY USE ONLY (Leave blank)	2. REPORT DATE	3. REPORT TYPE AND DATES COVERED
	November 1992	Technical Memorandum

4. TITLE AND SUBTITLE
Modal Element Method for Scattering of Sound by Absorbing Bodies

5. FUNDING NUMBERS
WU-505-62-52

6. AUTHOR(S)
Kenneth J. Baumeister and Kevin L. Kreider

7. PERFORMING ORGANIZATION NAME(S) AND ADDRESS(ES)
National Aeronautics and Space Administration
Lewis Research Center
Cleveland, Ohio 44135-3191

8. PERFORMING ORGANIZATION REPORT NUMBER
E-7126

9. SPONSORING/MONITORING AGENCY NAMES(S) AND ADDRESS(ES)
National Aeronautics and Space Administration
Washington, D.C. 20546-0001

10. SPONSORING/MONITORING AGENCY REPORT NUMBER
NASA TM- 106009

11. SUPPLEMENTARY NOTES
Prepared for the American Society of Mechanical Engineers Winter Annual Meeting, Anaheim, California, November 8-13, 1992. Kenneth J. Baumeister, NASA Lewis Research Center, Cleveland, Ohio, and Kevin L. Kreider, The University of Akron, Department of Mathematical Sciences, Akron, Ohio. Responsible person, Kenneth J. Baumeister, (216) 433-5886.

12a. DISTRIBUTION/AVAILABILITY STATEMENT
Unclassified - Unlimited
Subject Category 71

12b. DISTRIBUTION CODE

13. ABSTRACT *(Maximum 200 words)*

The modal element method for acoustic scattering from a two-dimensional body is presented. The body may be acoustically soft (absorbing) or hard (reflecting). The infinite computational region is divided into two subdomains – the bounded finite element domain, which is characterized by complicated geometry and/or variable material properties, and the surrounding unbounded homogeneous domain. The acoustic pressure field is represented approximately in the finite element domain by a finite element solution, and is represented analytically by an eigenfunction expansion in the homogeneous domain. The two solutions are coupled by the continuity of pressure and velocity across the interface between the two subdomains. Also, for hard bodies, a compact modal ring grid system is introduced for which computing requirements are drastically reduced. In this paper, analysis for two-dimensional scattering from solid and coated (acoustically treated) bodies is presented, and several simple numerical examples are discussed. In addition, criteria are presented for determining the number of modes to accurately resolve the scattered pressure field from a solid cylinder as a function of the frequency of the incoming wave and the radius of the cylinder.

14. SUBJECT TERMS

15. NUMBER OF PAGES
14

16. PRICE CODE
A03

17. SECURITY CLASSIFICATION OF REPORT	18. SECURITY CLASSIFICATION OF THIS PAGE	19. SECURITY CLASSIFICATION OF ABSTRACT	20. LIMITATION OF ABSTRACT
Unclassified	Unclassified	Unclassified	

NSN 7540-01-280-5500

Standard Form 298 (Rev. 2-89)
Prescribed by ANSI Std. Z39-18
298-102